Clustering in the Absence of Attractions: Density Functional Theory and Computer Simulations

Bianca M. Mladek,*,† Dieter Gottwald,† Gerhard Kahl,† Martin Neumann,‡ and Christos N. Likos§

Center for Computational Materials Science and Institut für Theoretische Physik, Technische Universität Wien, Wiedner Hauptstrasse 8-10, A-1040 Wien, Austria, Institut für Experimentalphysik, Universität Wien, Strudlhofgasse 4, A-1090 Wien, Austria, and Institut für Theoretische Physik II: Weiche Materie, Heinrich-Heine-Universität Düsseldorf, Universitätsstrasse 1, D-40225 Düsseldorf, Germany

Received: June 15, 2007; In Final Form: August 6, 2007

We numerically investigate the formation of stable clusters of overlapping particles in certain systems interacting via purely repulsive, bounded pair potentials. In close vicinity of a first-order phase transition between a disordered and an ordered structure, clusters are encountered already in the fluid phase which then freeze into crystals with multiply occupied lattice sites. These hyper-crystals are characterized by a number of remarkable features that are in clear contradiction to our experience with harshly repulsive systems: upon compression, the lattice constant remains invariant, leading to a concomitant linear growth in the cluster population with density; further, the freezing and melting lines are to high accuracy linear in the density−temperature plane, and the conventional indicator that announces freezing, that is, the Hansen−Verlet value of the first peak of the structure factor, attains for these soft systems much higher values than for their hard-matter counterparts. Our investigations are based on the generalized exponential model of index 4 (i.e., $\Phi(r) \sim \exp[-(r/\sigma)^4]$). The properties of the phases involved are calculated via liquid state theory and classical density functional theory. Monte Carlo simulations for selected states confirm the theoretical results for the structural and thermodynamic properties of the system. These numerical data, in turn, fully corroborate an approximate theoretical framework that was recently put forward to explain the clustering phenomenon for systems of this kind (Likos, C. N.; Mladek, B. M.; Gottwald, D.; Kahl, G. *J. Chem. Phys.* **2007**, 126, 224502).

1. Introduction

The tendency of particles to form stable clusters is a well-known feature of systems with long-range repulsions and short range attractions,[1−12] which, for example, are models for the competition between electrostatic and depletion forces in colloidal systems. However, when clustering behavior was also observed in computer simulations of certain systems interacting via bounded and purely repulsive pair potentials,[13] it did not receive due attention. Two reasons quite probably lie at the core of this initial lack of follow-up investigations of this kind of aggregation phenomenon: first, the fact that some general organizing principle was missing that would rationalize and put in physical context the appearance of clusters in the absence of attractions; and second, some 10 years ago, bounded potentials were viewed in general as rather academic, unrealistic model interactions without any correspondences in nature. Meanwhile, considerable progress in soft matter physics has cleared up the second objection. In numerous examples, it was shown that the concept of weakly diverging or bounded potentials is a realistic one if understood as effective interactions, for example, between polymeric macromolecules of low internal monomer concentrations, such as polymer chains,[14−16] dendrimers,[17,18] microgels[19−21] or block copolymers,[22,23] once the large number of degrees of freedom of the constituent monomeric entities have been averaged out via suitable methods (for an overview see ref 24). The phase diagrams of these systems exhibited new and surprising features that are in sharp contrast to the experience accumulated over a long time in the study of the phenomena typical of harshly repulsive systems. Apart from the clustering phenomenon, there is another, complementary type of phase behavior relevant in the context of the present work, that is, that of re-entrant melting accompanied by a maximum freezing temperature.[25−27] Here, the fluid upon compression crystallizes via a first-order phase transition for temperatures below an upper marginal temperature, and it remelts again as the density is further increased. Above the marginal temperature, no solid phase is found, and the fluid is stable at all densities.

It took several years until the results of ref 13 were put into a broader context within the scope of theoretical arguments.[28] A criterion was derived which allowed for the classification of the phase behavior of systems where particles interact via bounded, strictly positive interactions on the basis of the behavior of the potentials' Fourier transform (FT) as either the clustering or the re-entrant melting scenario. These investigations also explained why the Gaussian core model (GCM) shows re-entrant melting[25,26,29−34,37] while the penetrable sphere model (PSM)[38−46] exhibits clustering, though they are both bounded, purely repulsive potentials.

Another 5 years later, a consistent understanding of the phenomenon of clustering was obtained via detailed free energy calculations based both on density functional theory (DFT) and on computer simulations.[47,48] Moreover, these studies confirmed the theoretical results put forward in ref 28. Subsequently, we

* Corresponding author. Phone: +4315880113631. Fax: +4315880113699. E-mail: mladek@tph.tuwien.ac.at.
† Technische Universität Wien.
‡ Universität Wien.
§ Heinrich-Heine-Universität Düsseldorf.

10.1021/jp074652m CCC: $37.00
Published on Web 10/12/2007

recently proposed a very general theoretical concept that provided comprehensive understanding of the clustering phenomenon and revealed several striking properties of the cluster phase.[49]

In putting the clustering and crystallization scenario of ref 28 to a strict test, several aspects of the statistical mechanics of the system have to be treated with particular care, since the possibility of aggregation introduces additional complications. First, the candidate crystal phases have to be identified in an unbiased fashion, since packing arguments, which are usually evoked for harshly repulsive interactions and which favor the typical fcc-periodic arrangement, do not dictate the physics for soft interactions.[50] Second, by changing the number of particles occupying a lattice site, clustering offers an additional possibility to adjust and optimize the lattice constant of the crystal phases. Thus, the latter becomes a variational parameter in the free energy of the solid. Therefore, it is an intricate task to determine the free energies of the different phases with sufficient accuracy to be able to obtain the phase boundaries correctly. Finally, the width of the particle oscillations around lattice sites as well as the distribution of cluster sizes in the crystal have to be determined. The purpose of this work is to address in detail the issues mentioned above and to elucidate thereby the salient physical mechanisms leading to cluster formation for a whole class of repulsive and bounded interaction potentials. The above-mentioned, recently proposed analytical approach to the problem of clustering and crystallization of such potentials[49] shed light into the general underlying mechanisms present in these systems, but the framework rested on a simplifying assumption: in writing the expression for the free energy of the crystal phase as a sum of contributions from the modes with wavenumbers given by the crystal's reciprocal lattice vectors (RLV), only the first nonvanishing one was kept in the sum. Here, a full minimization of the density functional is performed instead, and in this way, the role of all of the RLV shells of the solid is brought forward. It is seen that these cause a transition from the bcc to the fcc arrangement at sufficiently high densities, which is not predicted by the simplified theory of ref 49. A short account of the present work has been presented in ref 47.

The rest of the paper is organized as follows: after introducing in section 2 the specific model whose phase diagram and clustering properties we want to investigate, we briefly present in section 3 the theoretical schemes that we require to calculate the properties of the fluid and of the ordered cluster phases. To put the results from theory to the test, we performed MC simulations, whose implementation details are explained in section 4. The subsequent section is devoted to a thorough discussion of the results, and the paper is closed by a summary of the results and outlook in section 6.

2. Model

Our investigations are focused on the generalized exponential model of index n (GEM-n). This is a family of bounded, purely repulsive soft model systems defined by the spherically symmetric pair potential

$$\Phi(r) = \epsilon \exp[-(r/\sigma)^n] \tag{1}$$

where ϵ and σ are the model's characteristic energy and length scales. The non-negative parameter n tunes the steepness of the repulsion and allows us to consider a whole range of potentials that includes not only the GCM for $n = 2$, but also the PSM for $n \to \infty$ as special cases.

On the basis of the behavior of the structure factor, $S(q)$, within the scope of a mean field approximation, Likos et al.[28] proposed a criterion that provides information about the topology of the phase diagram of systems with bounded, purely repulsive interactions. It states that if the FT, $\tilde{\Phi}(q)$, is a positive semidefinite, monotonically decaying function, the potential belongs to the so-called Q^+ class, and the system will show re-entrant melting behavior upon compression. If, on the other hand, $\tilde{\Phi}(q)$ exhibits oscillatory behavior and thus attains negative values for certain ranges of q, the potential is a $Q^\pm$ potential. Such systems will show clustering, and the system will freeze at all temperatures into a hyper-crystal with multiply occupied lattice sites. Applying this criterion to the GEM-n family, one can show the following (for a proof cf. Appendix A of ref 49):

(i) For $n \leq 2$, $\tilde{\Phi}(q) > 0$ for all q, and we therefore expect the re-entrant melting scenario for this index range. The phase diagram of the GCM, which represents the limiting case $n = 2$, does in fact show this topology.[26,32]

(ii) For $n > 2$, $\tilde{\Phi}(q)$ oscillates, thereby delimiting the index range where we expect clustering behavior. The PSM, for which clustering was already documented in a previous contribution[38] and which is recovered for $n \to \infty$, is a representative of this class.

In this work, we restrict our investigations to $n = 4$ in an effort to investigate the clustering phenomenon in detail by means of a typical example for positive potentials with a negative minimum (located at q_*) in its FT. We then compare our results to the theoretical predictions presented in ref 49.

Up to now, the effective interactions determined for the various macromolecular systems already mentioned in the introduction[14−23] all showed re-entrant melting behavior, and some even took the functional form of a GCM (i.e., a GEM-2).[16,17] In work under way, however, we have succeeded in computationally designing amphiphilic dendrimers whose effective pair interactions show a functional form that can be approximated very accurately with a GEM-n potential with index $n \cong 3.1$,[51] that is, well within the $Q^\pm$ range. Since experimental realization of clustering systems is still missing, we hope that this work as well as the results presented here will serve as a motivation and useful guide to experimentalists of how to assemble macromolecules in the lab such that their effective interactions belong to the $Q^\pm$ class.

3. Theory

Since our main aim is to determine the phase diagram of the GEM-4, we have to choose appropriate methods to determine the free energies of the different states of matter involved, that is, the fluid and the ordered cluster phases. For the latter ones, we moreover need a reliable search algorithm that identifies the crystalline candidate structures in an unbiased way.

3.1. Fluid Phase. We decided to calculate the properties of the fluid phase within the mean field approximation (MFA), a choice based on the theoretical background explained in ref 49. For potentials lacking a hard core, the MFA ansatz for the direct correlation function, $c(r)$,

$$c(r) = -\beta\Phi(r) \text{ for all } r \tag{2}$$

is used as a closure to the Ornstein−Zernike (OZ) equation,[52]

$$h(r) = c(r) + \rho \int d\mathbf{r}' h(r') c(|\mathbf{r} - \mathbf{r}'|) \tag{3}$$

where $h(r)$ is the total correlation function, $\beta = (k_B T)^{-1}$ is the inverse temperature, and ρ is the number density. Equations 2 and 3 are solved numerically.

The thermodynamic properties of the fluid phase are then calculated via the energy route, which relates the excess internal

energy per particle, $U^{ex}/N \equiv u^{ex}(\rho,\beta)$, to the radial distribution function (RDF), $g(r) = h(r) + 1$, via

$$\frac{U^{ex}}{N} = 2\pi\rho \int_0^\infty dr r^2 g(r)\Phi(r) \quad (4)$$

where the RDF is ρ and β dependent. An additional integration over β leads to the excess free energy per particle, $F^{ex}/N \equiv f^{ex}(\rho, \beta)$,

$$\beta f^{ex}(\rho, \beta) = \int_0^\beta d\beta' u^{ex}(\rho, \beta') \quad (5)$$

Where, in an exact closure, the virial, compressibility, and energy routes to the free energy would provide identical results,[52] the approximate nature of the MFA leads to different ones; that is, it suffers, as most closures do, from thermodynamic inconsistency. We opted for the energy route because it delivers the most accurate results in comparison with simulation (see section 5).

3.2. Ordered Cluster Phases. The description of the properties of the solid phases is more delicate. A priori we do not know which ordered structures the cluster phases will form in equilibrium. In an effort to circumvent the arbitrariness inherent to conventional approaches, we have solved the problem by using a genetic algorithm (GA),[53] that is, a tool which searches among all possible lattices for the equilibrium structure. For successful applications of this convenient and reliable tool, we refer to refs 20, 21, and 53.

The basic idea of the GA can be outlined as follows: in an initial step, we consider a large number of randomly generated possible candidate structures, termed individuals, which form a so-called (first) generation. A fitness value is assigned to each individual which is a measure of its quality in the sense that a better solution has a higher fitness value. In our case, we require that a lower free energy of a lattice corresponds to a higher fitness value. Next, suitable pairs of parents are chosen according to their fitness, and via recombination, they create the individuals (lattice structures) of the subsequent generation. With a certain probability, these individuals are then subject to a mutation process. We proceed in this way for a sufficiently long sequence of generations, keeping track of the individual with the highest fitness value, that is, the lattice structure with the lowest free energy so far. In general, the algorithm converges rapidly toward the equilibrium structure for a given state point. For conceptual details, we refer to ref 53.

In our particular problem, the GA searches for the optimum ordered cluster structures at $T = 0$, which are then considered as candidates for the phase diagram at finite temperatures. At $T = 0$, the cluster phase has ideal properties: all clusters are populated by the same number of particles, denoted as n_c, which sit perfectly on top of each other at the positions of an ideal lattice. Our measure of fitness is related to the free energy, F, which at $T = 0$ is identical to the internal energy, U, and is given by

$$\frac{F(T=0)}{N} = \frac{U}{N} = \frac{n_c - 1}{2}\Phi(\mathbf{R}=0) + \frac{n_c}{2}\sum_{\mathbf{R}\neq 0}\Phi(\mathbf{R}) \quad (6)$$

where $\{\mathbf{R}\}$ denotes the set of Bravais lattice vectors of a candidate structure for the cluster phase. Here, the first term is the interaction energy of a particle with the $(n_c - 1)$ particles of the same cluster, while the second one describes the interaction with the other clusters of the crystal. In employing the GA, we minimized the lattice sum per particle, U/N, with respect to both the Bravais lattice and the cluster occupation number n_c. Strictly speaking, at $T = 0$, n_c can only assume integer values, if we insist that each site is occupied by an identical number of particles; however, rational values of n_c arising from populating different sub-lattices with different integer occupation numbers and periodically repeating the pattern are in principle also allowed. In our calculation, we avoided these cases by employing a kind of mean-field approach: possible corrections to the lattice sum from short-range correlations that lead to differently populated sub-lattices were ignored, and the occupation number of all sites was set equal to the average value $\langle n_c\rangle$, a general real number. In reality, irrational occupations are, of course, forbidden for a ground state, pointing to the possibility of phase separation between optimally occupied states with rational occupation. However, at finite temperatures, it is expected that hopping processes will allow for the migration of particles and lead to an equalization of the average number $\langle n_c\rangle$ of particles on every site. Our approximation of setting $n_c = \langle n_c\rangle$ is expected to be valid for temperatures that are low enough, so that the entropic contribution, $-TS$, associated with the hopping processes, can be ignored in comparison with the lattice energy, U, in the expression $F = U - TS$ for the free energy F. Moreover, since we do not expect sub-lattices to be populated by vastly different particle numbers even at $T = 0$, the error we make in replacing n_c by $\langle n_c\rangle$ is very small, and the approach offers reliable information on the possible crystal structures at $T = 0$.

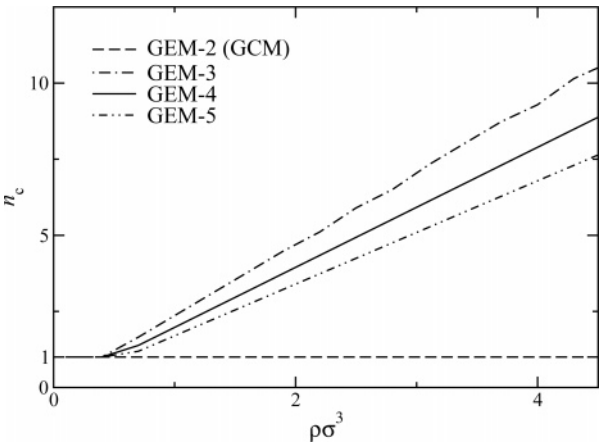

Figure 1. Cluster size n_c as a function of $\rho\sigma^3$ for different index values n of the GEM-n potentials as predicted by the GA. As we can see, $n_c = 1$ for all densities in the case of the GCM. The small fluctuations in the data of the GEM-3 stem from the fact that the free energy differences between fcc and bcc are so small that the GA has difficulties in deciding unambiguously between the competing structures.

Determining the zero-temperature phase diagram for the GEM-n family for various potential indices n via the GA, we find that, for $n > 2$, only fcc and bcc lattices appear, a result that is in full agreement with the predictions in ref 49. This also seems to indicate that the effective cluster−cluster interactions are harshly repulsive, a typical feature for systems that freeze in fcc and bcc solids, such as, for example, the Lennard-Jones fluid. As we see from Figure 1, for $n = 2$ (the Gaussian core model), the GA yields conventional crystals consisting of singly occupied sites, in agreement with the exact calculations of Stillinger.[34] For low densities $\rho\sigma^3 \lesssim 0.2$, the GA predicts fcc to be the stable phase which is in agreement with the results obtained by Stillinger in ref 34 which predicts this phase for $\rho\sigma^3 < \pi^{-3/2} \sim 0.18$. For higher densities, we find the bcc structure.

From the GA results, we see that for the densities considered ($0.2 < \rho\sigma^3 < 10$) the bcc structure is dominant for n values

close to the clustering threshold value $n = 2$, while for larger n, that is, $n \gtrsim 3$, fcc becomes more favorable. At the boundary between the two regimes ($n \sim 3$), the energy difference between the two structures is vanishingly small, resulting in the GA having considerable difficulties to decide unambiguously between the competing structures in this particular situation,[53] which is also reflected in the small fluctuations in the data of the GEM-3 in Figure 1. For all $n > 2$ considered, the GA predicts $n_c > 1$, which is displayed in Figure 1. In ref 49, it has been shown that n_c is proportional to ρ/q_*, where q_* is the value of the wavenumber for which $\tilde{\Phi}(q)$ has a minimum. The results of Figure 1 fully confirm this proportionality relation. The slope of the $n_c(\rho)$ versus ρ lines indeed decreases with n since q_* grows with n, as can be easily checked numerically.

With the possible candidate structures at hand, we can now proceed to finite temperatures where it is most convenient to describe the ordered cluster phases within the framework of the classical density functional theory (DFT).[35,36] As justified explicitly in ref 49, we use a mean-field format for the free energy functional $\mathcal{F}[\rho]$,

$$\mathcal{F}[\rho] = \mathcal{F}_{\mathrm{id}}[\rho] + \mathcal{F}_{\mathrm{ex}}[\rho] \tag{7}$$

where the ideal part $\mathcal{F}_{\mathrm{id}}[\rho]$ is given by

$$\mathcal{F}_{\mathrm{id}}[\rho] = k_{\mathrm{B}}T \int \mathrm{d}\mathbf{r}\rho(\mathbf{r})\{\ln[\rho(\mathbf{r})\Lambda^3] - 1\} \tag{8}$$

with Λ being the de Broglie wavelength, and the excess part, $\mathcal{F}_{\mathrm{ex}}[\rho]$, is obtained via

$$\mathcal{F}_{\mathrm{ex}}[\rho] = \frac{1}{2}\int \mathrm{d}\mathbf{r}_1 \int \mathrm{d}\mathbf{r}_2 \rho(\mathbf{r}_1)\rho(\mathbf{r}_2)\Phi(|\mathbf{r}_1 - \mathbf{r}_2|) \tag{9}$$

For the inhomogeneous density field, $\rho(\mathbf{r})$, we use a periodic array of Gaussian cluster density profiles

$$\rho_{\mathrm{cl}}(\mathbf{r}) = n_c\left(\frac{\alpha}{\pi}\right)^{3/2} \mathrm{e}^{-\alpha\mathbf{r}^2} \tag{10}$$

localized at the lattice sites $\{\mathbf{R}\}$, that is,

$$\rho(\mathbf{r}) \equiv \sum_{\{\mathbf{R}\}} \rho_{\mathrm{cl}}(\mathbf{r} - \mathbf{R}) = n_c\left(\frac{\alpha}{\pi}\right)^{3/2} \sum_{\{\mathbf{R}\}} \mathrm{e}^{-\alpha(\mathbf{r}-\mathbf{R}^2)} \tag{11}$$

Our choice of this particular shape for the density profiles was anticipated in ref 49 and will be justified a posteriori when comparing the theoretical data with the simulation results (see section 5). The inhomogeneous density field $\rho(\mathbf{r})$ is uniquely determined by two parameters characterizing the cluster density profiles, that is, the width α of the profile and the cluster occupancy number or cluster size, n_c. Minimizing the functional given by eqs 7−9 with respect to both α and n_c at fixed ρ and T gives us the theoretical predictions for the equilibrium values of α and n_c.

Inserting the ansatz (eq 11) into eqs 7−9, the functional $\mathcal{F}[\rho]/N$ reduces to a function $f = f(n_c, \alpha)$ that can be split into an ideal, an inter-, and an intra-cluster contribution

$$f(n_c, \alpha) = f_{\mathrm{id}}(n_c, \alpha) + f_{\mathrm{inter}}(n_c, \alpha) + f_{\mathrm{intra}}(n_c, \alpha) \tag{12}$$

For the ideal contribution, we find

$$f_{\mathrm{id}}(n_c, \alpha) = k_{\mathrm{B}}T\,[\ln n_c + 3/2\,\ln(\alpha\sigma^2/\pi) - 5/2 + 3\ln(\Lambda/\sigma)] \tag{13}$$

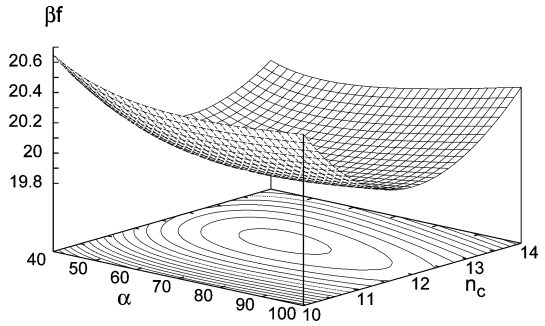

Figure 2. $\beta f(n_c, \alpha)$ given by eq 12 as a function of n_c and α for a GEM-4 system at $k_{\mathrm{B}}T/\epsilon = 0.5$ and $\rho\sigma^3 = 6$ in the fcc phase.

which is an excellent approximation to the ideal free energy, provided that the Gaussians in eq 11 do not overlap, which is the case for $\alpha\sigma^2 \gtrsim 30$, representing thus a physically reasonable lower bound for α. Here, we take σ as a typical scale for the nearest-neighbor distance d in the lattice; as will be shortly confirmed, the values we obtain in the case of the GEM-4 for the different solid phases are $d \cong 1.4\sigma$.[47] The inequality $\alpha\sigma^2 \gtrsim 30$ thus corresponds to $\alpha d^2 \gtrsim 60$, for which the degree of overlap between neighboring Gaussians is indeed negligible. Note also that from eqs 8 and 11 it is easy to see that for $\alpha \to 0$ the ideal free energy per particle tends to $k_{\mathrm{B}}T[\ln(\rho\Lambda^3) - 1]$, the finite free energy of the ideal gas, whereas the approximate expression of eq 13 has a negative, logarithmic divergence there, signaling the breakdown of the approximation for low α values.

Further, for the other two terms in eq 12, we find

$$f_{\mathrm{inter}}(n_c, \alpha) = n_c\sqrt{\frac{\alpha}{8\pi}} \times \sum_{\mathbf{R}\neq 0} \int_0^\infty \mathrm{d}r\,\frac{r}{R}\,[\mathrm{e}^{-\alpha(r-R)^2/2} - \mathrm{e}^{-\alpha(r+R)^2/2}]\Phi(r) \tag{14}$$

and

$$f_{\mathrm{intra}}(n_c, \alpha) = (n_c - 1)\sqrt{\frac{\alpha^3}{2\pi}} \int_0^\infty \mathrm{d}r\, r^2\, \mathrm{e}^{-\alpha r^2/2}\Phi(r) \tag{15}$$

In eq 14, R denotes the modulus of the Bravais lattice vector $\mathbf{R}$. For a given density ρ, the modulus of the lattice vectors depends on the degree of clustering n_c, since the elementary cell can expand by accumulating more particles per lattice site. In Figure 2, we show for a particular state point of the GEM-4 system the typical dependence of $f(n_c, \alpha)$ on n_c and α. It can be seen that the surface takes the shape of a trough that runs parallel to the α axis; that is, for each α, the minimum with respect to n_c is located at an n_c value that is α independent. This is connected with the tendency of the system to adjust its lattice constant in such a way that the modulus of the first shell of RLVs coincides with the value q_* at which $\tilde{\Phi}(q)$ attains its negative minimum and confirms the analytical results of ref 49.

A detailed consideration of the separate contributions to $f(n_c, \alpha)$, given by eqs 13−15, as functions of n_c at fixed α and shown in Figure 3 offers the key to understand the existence of stable, finite clusters in this system. On increasing n_c, the lattice constant widens, the values of R in eq 14 grow, and expensive close contacts with nearest neighbor clusters are avoided as shown by the fact that $f_{\mathrm{inter}}(n_c)$ drops monotonically with n_c. On the other hand, the entropy loss due to particle aggregation, expressed by the term $\ln n_c$ in eq 13, and the self-interaction within the cluster, given by eq 15, both disfavor the formation

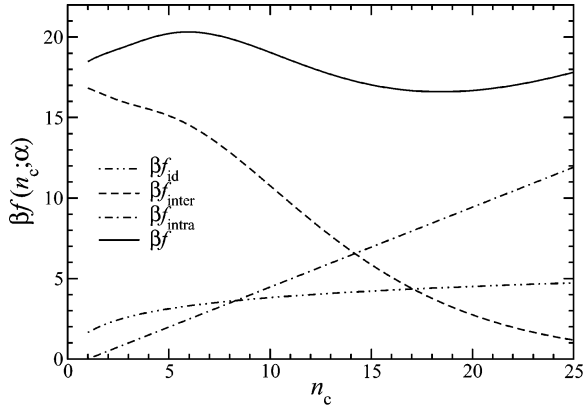

Figure 3. Contributions to $\beta f(n_c; \alpha)$ according to eqs 13−15 as functions of n_c for an fcc crystal formed in a GEM-4 system at $k_BT/\epsilon = 1$, $\rho\sigma^3 = 9$, and $\alpha\sigma^2 = 45.51$, i.e., the $\alpha\sigma^2$ that minimizes the free energy. The minimum in $\beta f(n_c; \alpha)$ is found at $n_c \sim 18.4$.

of clusters which can be seen from the monotonic increase of the respective terms with n_c. On the other hand, very large values of n_c are unlikely because, at constant particle density, this would reduce the cluster density to such an extent that even the (cluster) nearest neighbor distance moves outside the range of the potential $\Phi(r)$. At this point, the entropic and self-interaction terms dominate and stop further aggregation. The interplay of these two competing contributions, the intracluster interaction and entropy, on the one hand, and the intercluster contribution, on the other hand, lead to an overall $f(n_c, \alpha)$ which shows a global minimum at a finite value of $1 < n_c < \infty$, representing the optimal, equilibrium cluster size for this state point and rendering the clusters stable both against decomposition ($n_c = 1$) and unlimited growth ($n_c \rightarrow \infty$). Uncontrollable growth of n_c would be unfavorable not only on the basis of thermodynamic arguments presented above but also on more fundamental, mechanical stability grounds. Indeed, should n_c and, correspondingly, the lattice constant, grow too large, there would be no appreciable restoring force from neighboring clusters to provide the stabilization mechanism for small lattice oscillations, and the crystal would lose its ordered structure.

4. Simulation

To put the theoretical results to the test, we performed Monte Carlo (MC) simulations of the GEM-4 system in the canonical ensemble, that is, at fixed particle number N, volume V, and temperature T. While in simulations of systems that freeze into singly occupied crystals ~500 particles already provide sufficiently reliable results, the situation is completely different in systems where clustering transitions may occur. In this case, to guarantee a sufficiently large number of *clusters*, we need considerably more particles in our simulation volume, rendering the use of conventional MC techniques computationally rather expensive where the determination of the distance between particles and the evaluation of the potential energy of a given particle configuration is the most time-consuming part.

Therefore, we had to speed up our MC simulations to make them feasible for systems that show clustering transitions. Motivated by the considerations in refs 54, 55, and 48, we implemented lattice Monte Carlo (LMC) simulations, a technique originally proposed by Panagiotopoulos.[56] The central idea of LMC is to transform the continuous system into a lattice model by restricting the possible particle positions within the simulation box to a finite number of discrete coordinates. As a consequence, there is only a finite number of possible distances between pairs of particles. Assuming that the particles' interaction is translationally invariant, these distances can be stored in a lookup table which only needs to be determined once at the beginning of the simulation. We decided to discretize the cubic simulation box via a grid of 2^b possible positions along each dimension, b being an integer number. Analysis of the discretization errors, which are described in detail in refs 54 and 55, indicate that $b = 8$ is sufficient to reproduce the results of conventional MC simulations. In addition, we also implemented the cell list method to speed up the simulations even further.[57]

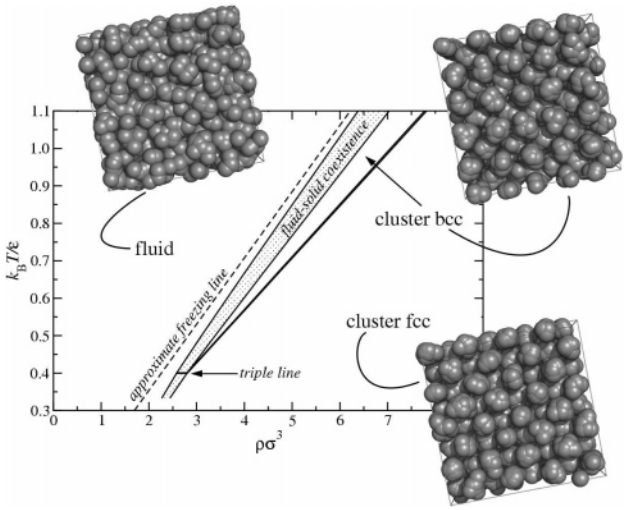

Figure 4. Theoretical prediction for the phase diagram of a GEM-4 system (as discussed in the text). The solid lines are the coexistence lines. We also show three snapshots of the system obtained from MC simulations at $k_BT/\epsilon = 1.1$ for the fluid phase ($\rho\sigma^3 = 6$), the cluster bcc phase ($\rho\sigma^3 = 7.5$), and the cluster fcc phase ($\rho\sigma^3 = 8.5$). Note that for the two higher densities, every lattice site is multiply occupied. The particle diameters are not to scale and were chosen arbitrarily to optimize visibility.

5. Results

We start the discussion of our results by showing the theoretical prediction for the phase diagram based on the MFA and DFT results, depicted in Figure 4. To give a qualitative understanding of the clustering phenomenon, we also show three simulation snapshots in the same figure, all taken at the same temperature, that is, $k_BT/\epsilon = 1.1$, but at different densities and in different phases. The explicit values for the densities are $\rho\sigma^3 = 6$, where the system is evidently in the fluid phase, $\rho\sigma^3 = 7.5$ for the cluster bcc and $\rho\sigma^3 = 8.5$ for the cluster fcc phase.

In the following, we will focus on the different phases encountered in Figure 4 and explain in detail how we determined the phase diagram. We start by analyzing the disordered, homogeneous phase. For $\rho\sigma^3 = 6$ and $k_BT/\epsilon = 1.1$, the system is already very close to the DFT prediction of the freezing line (cf. Figure 4). A closer investigation of the particle positions shows that the fluid phase is actually a mixture of strongly aspherical clusters of particles with a vast variation of cluster sizes, n_c. Turning to the RDF in Figure 5, we see that upon increasing the density, the value of $g(0)$ starts to rise. This maximum, which is also present in the fluid's RDF, indicates that particles indeed agglomerate to clusters already in the liquid phase. In a system where particles interact via a continuous potential, it is of course not possible to unambiguously define a cluster in the fluid phase. As we show in the inset of Figure 5, the RDF does not completely vanish at its first minimum for this particular state point and thus only gives an indication of

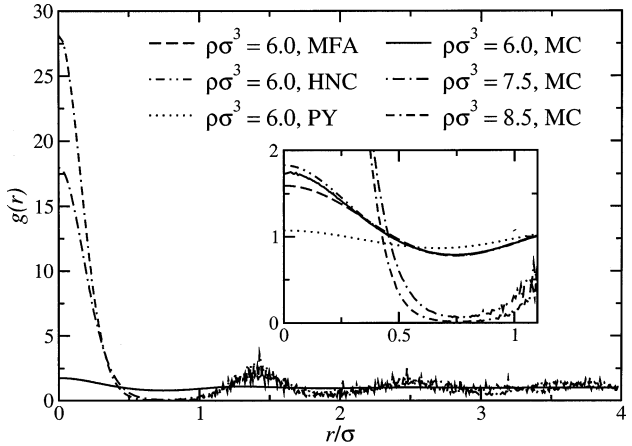

Figure 5. $g(r)$ as a function of r/σ for a GEM-4 system at $k_BT/\epsilon = 1.1$ as determined from MC simulations of the states shown in the snapshots in Figure 4. For the fluid phase at $\rho\sigma^3 = 6$, results from MFA, HNC, and PY are shown in the inset. We want to stress that the fluctuations seen in the data of the two highest densities are characteristic of LMC results for solid systems.

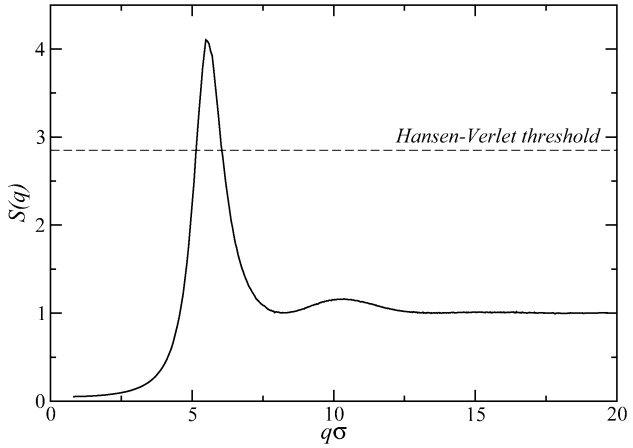

Figure 6. Structure factor $S(q)$ as a function of $q\sigma$ as obtained by MC simulations for a fluid GEM-4 system close to freezing, i.e., at $k_BT/\epsilon = 1.1$ and $\rho\sigma^3 = 6$. The value of the first peak of $S(q)$ is considerably higher than the Hansen−Verlet threshold value that indicates freezing in harshly repulsive systems.

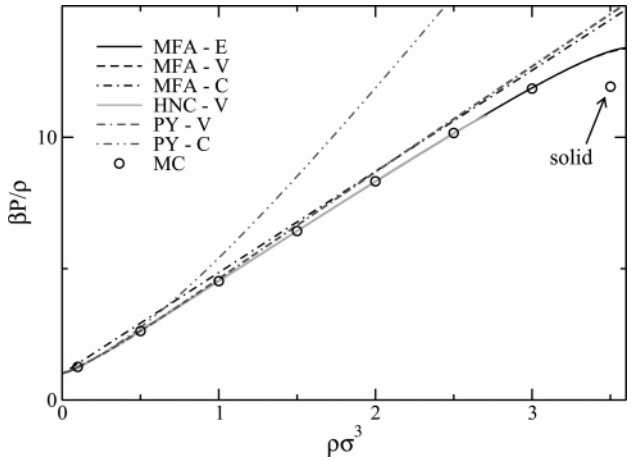

Figure 7. Reduced, dimensionless pressure, $\beta P/\rho$, as a function of $\rho\sigma^3$ for the GEM-4 at $k_BT/\epsilon = 0.5$, calculated via different thermodynamic routes (V, virial; C, compressibility; and E, energy route) and using various liquid state theories.[52] MC simulation data are given by the symbols. While PY fails to reliably reproduce the simulation data especially at high densities, HNC initially provides a reasonable approximation but fails to converge well before the system crystallizes for densities around $\rho\sigma^3 \sim 3$. This leaves the energy route of the MFA as the best option to describe the properties of the fluid. Note that the MC data point at the highest density already corresponds to the solid phase.

the spatial extent of the clusters. However, as soon as the system freezes, the space between two clusters becomes nearly depleted, thereby allowing for a definition of the extent of a cluster. The cluster size, n_c, can then either be defined by integration over the first peak of $4\pi r^2\rho g(r)$ up to the first minimum of $g(r)$ or via a cluster analysis, where the location of this first minimum is used as a limiting value to group particles in clusters. The inset of the same figure shows that the depopulated region becomes broader as ρ is increased, which reflects the tendency that at higher densities an increasing potential energy barrier between the clusters drives particles out of these interstitial regions and into the clusters. Such a behavior seems completely counter-intuitive since this formation of stable clusters occurs at the complete absence of attraction. Nevertheless, it can be understood by considering the fact that full overlaps of particles create additional space for the clusters, offering thus the system a possibility to increase its entropy. Moreover, above the overlap density, even an energetic gain may be achieved, since a single full overlap could be less expensive than the sum of the costs of the partial overlaps with the ∼12 neighbors in a highly coordinated, dense fluid. This is immediately evident in the case of the PSM, for which the energy cost is independent of separation once the particles overlap. A detailed account of these contributions for the PSM is given in ref 38 in real space, whereas a more general argument based on reciprocal-space considerations can be found in ref 49.

In Figure 6, we show the structure factor, $S(q)$, for the fluid phase according to MC simulations. We see that the first peak considerably exceeds the value of 2.85, which, according to the Hansen−Verlet criterion,[58,59] indicates the freezing transition in harshly repulsive fluids. This demonstrates that the GEM-4 system can sustain a higher degree of spatial correlations than hard matter systems before it freezes. Note that at this density the fluid phase is indeed the stable one, since crystalline initial configurations spontaneously lose their order and melt during the course of the simulations.

Although the MFA does not capture the structural properties of clustering in the fluid phase on a quantitative level, it turns out that it can reproduce the increase in $g(0)$ on a qualitative level, which we show in the inset of Figure 5. As we can see there, this feature is also predicted by the hypernetted chain (HNC) or the Percus Yevick (PY) approximations[52] with different levels of success. Moreover, the thermodynamic results obtained via the MFA energy route agree very well with results of computer simulations. To visualize this, we present as an example in Figure 7 the data for the reduced, dimensionless pressure, $\beta P/\rho$, for the GEM-4 at a rather low temperature of $k_BT/\epsilon = 0.5$. To put the success of the energy route of the MFA into a broader context, we also show in the same figure results calculated from MFA via different thermodynamic (i.e., energy, virial, or compressibility) routes, as well as using other liquid state theories, such as HNC or PY.[52] We see that PY fails to reliably reproduce the simulation data especially at high densities. HNC, on the other hand, performs very well but breaks down, that is, where $g(0) \gtrsim 1$ and well before the actual transition to a cluster solid. The results of the virial and energy route of MFA lie on top of those of the virial route of HNC, while the data of the compressibility route of MFA are in the vicinity of the virial route results of PY. Thus, despite being the simplest among the various closures to the OZ equation, the MFA surpasses all other closures since results can still be

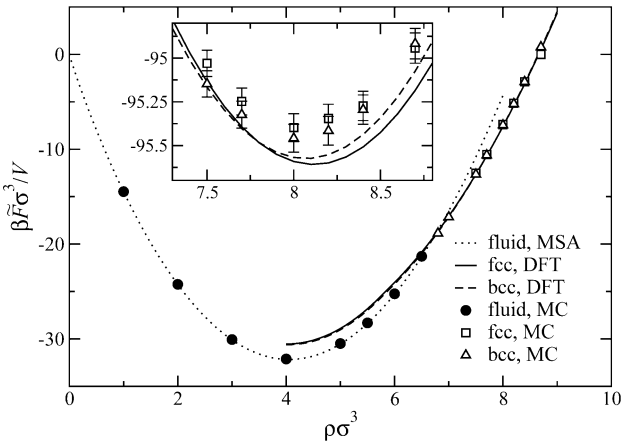

Figure 8. DFT and MC results for the modified free energy density $\beta\tilde{F}\sigma^3/V \equiv \beta F\sigma^3/V + K\rho\sigma^3$ of the GEM-4 system as function of $\rho\sigma^3$ at $k_BT/\epsilon = 1.1$. A term $K\rho\sigma^3$, irrelevant for the determination of the coexistence densities, has been added for clarity of presentation. The error bars of the MC results in the main plot are smaller than the symbol size. Inset: a close-up on the region of the bcc−fcc transition. Here, a different linear term $K\rho\sigma^3$ has been added to the free energies.

obtained when approaching the freezing transition. Note that at higher temperatures MFA is similarly accurate as the HNC in reproducing the data of simulations, as was shown in ref 49. All of these considerations leave the energy route of MFA as the best option to describe the properties of the fluid. A more detailed analysis of MFA data in direct comparison with computer simulation results can be found in ref 60 for several values of potential index n.

Thus, we are now able to calculate the free energy of the fluid via MFA and those of the competing solid structures, that is, fcc and bcc, via DFT as discussed in subsection 3.2. In Figure 8, we show the modified free energy density, $\beta\tilde{F}\sigma^3/V \equiv \beta F\sigma^3/V + K\rho\sigma^3$, for the fluid and the two cluster solid phases as a function of density at fixed temperature $k_BT/\epsilon = 1.1$. The term $K\rho\sigma^3$ was added to enhance visibility, but it is irrelevant for the determination of the coexistence densities. In the same figure, we also show data from MC simulations, where we determined the free energy via Widom's particle insertion method.[57,61] In the case of bounded potentials, this also works for the solid phases since, in contrast to harshly repulsive potentials, overlaps of particles only cost a finite amount of energy. As we see in Figure 8, the MC results are in good agreement with the DFT data. However, from this figure, it is also apparent how small the energy differences between the competing solid cluster phases are. Because of the size of the present error bars, it is therefore not possible to determine the exact location of the phase transition via conventional MC simulations. For this, more sophisticated simulation techniques of higher precision, using, for example, thermodynamic integration, are needed, which go beyond the scope of this paper.[62] Yet, in the MC simulations performed so far, we have observed that, for densities smaller than the DFT freezing density, crystals are not stable and spontaneously melt, which supports the basic validity of the DFT data. Also, our free energy MC data seem to indicate that the true bcc-fcc phase transition may be slightly shifted to higher densities compared to the DFT results.

Therefore, Figure 4 only shows the theoretical prediction of the phase diagram, which was obtained from the free energy curves via the common tangent construction and which we are going to discuss on a more quantitative level in the following. The approximate, analytical theory of ref 49 predicts for the freezing line (f) a straight line of the form:

$$\frac{k_BT_f}{\epsilon} = 1.393|\bar{\Phi}(q)|\rho_f\sigma^3 \approx 0.177\rho_f\sigma^3 \qquad (16)$$

where $|\bar{\Phi}(q)| \equiv |\tilde{\Phi}(q)|/(\epsilon\sigma^3) \cong 0.127$ is the absolute value of the negative minimum of the FT of the GEM-4 potential. Plotting eq 16 in the phase diagram, we see that it is reasonably close to the coexistence line predicted by the present, full numerical MFA and DFT calculations, which lead to an almost straight line that can be fitted by

$$\frac{k_BT_f}{\epsilon} = 0.186(1)\rho_f\sigma^3 - 0.080(5) \qquad (17)$$

Thus, eq 16 slightly overestimates the region of stability of the solid because it neglects contributions from RLVs which are positive, resulting thereby in an artificial lowering of the crystal's free energy.

Upon compression, the system undergoes a first-order transition into a cluster bcc phase, which occupies a wedge like shape in the (T, ρ) plane. As the density is further increased, the system exhibits another first-order transition into the cluster fcc phase which remains stable for all higher densities. The coexistence region between the two ordered structures is very narrow and not visible on the scale of Figure 4. Furthermore, MFA and DFT predict that, at $k_BT/\epsilon \cong 0.4$, the liquid and the two-ordered cluster phases coexist at a triple point. Below this temperature, the bcc phase vanishes, and the liquid freezes directly into the now thermodynamically more favorable cluster fcc crystals. As was already shown in ref 28, the mean field assumption, which both the MFA and the DFT rest upon, breaks down at very low temperatures. Therefore, using the present methods, no reliable prediction about the location of the phase boundaries can be made for this region of the phase space. Instead, one might proceed along the lines of Stillinger's treatment of the Gaussian core model[25,29,30] and perform a mapping of the Boltzmann factor of the system onto that of hard spheres. Defining an effective, density-dependent hard sphere diameter and using the known results for the freezing of hard spheres, the freezing boundaries for $T \to 0$ could be determined. This, however, lies beyond the scope of the present work.

As noted above, because of the magnitude and the overlap of the error bars of our MC free energy results, there are certain density ranges where we cannot, at present, decide whether fcc or bcc is the stable crystalline phase. Still, because of the similarity between the data of most properties of the two phases, MC simulations are indispensable to gain deeper insight into the clustering phenomenon, since they provide the connection between the microscopic details of the system and the mean field assumptions of the various theories involved. In the rest of the discussion, we either will present MC data for those solid phases predicted by DFT in cases where the effect discussed is independent of the actual crystal structure or will show data for both phases for all other cases.

On the basis of the data gathered for the three states corresponding to the simulation snapshots in Figure 4, we show in Figure 9 how the cluster size distribution changes at fixed temperature when compressing the system. As already mentioned before, in the fluid, the cluster size distribution is very broad, also because of the complications to define clusters in an unambiguous manner. For the bcc structure encountered at intermediate densities, the distribution of cluster sizes is already considerably narrower than in the fluid, and the mean occupancy number has also increased. In the fcc phase at $\rho\sigma^3 = 8.5$, a detailed study of the centers of mass of the clusters shows that the structure is less distorted than the bcc structure at

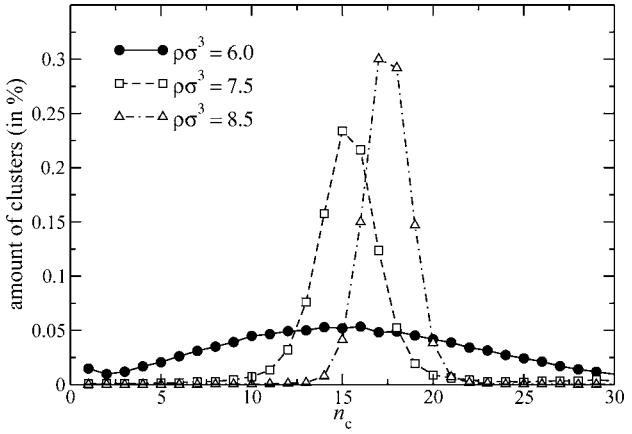

Figure 9. Distribution of cluster size n_c as obtained from MC simulations of the three states of the GEM-4 system shown in Figure 4 (i.e., at $k_BT/\epsilon = 1.1$). With increasing density, the maximum of n_c shifts to higher values, and the distribution becomes narrower.

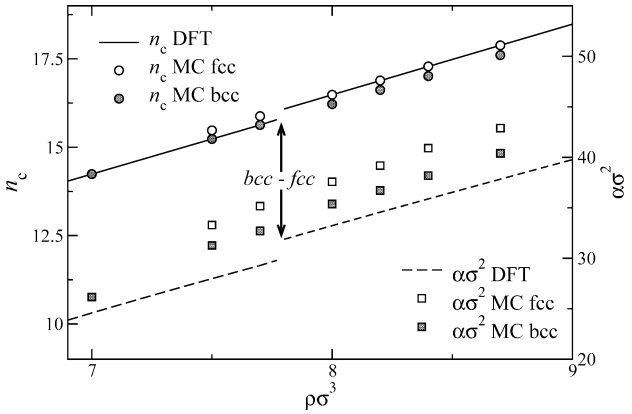

Figure 10. n_c and $\alpha\sigma^2$ as functions of $\rho\sigma^3$ for the GEM-4 systems at $k_BT/\epsilon = 1.1$. Discontinuities of both quantities at the density of the first-order bcc−fcc phase transition are visible. Lines, DFT results; symbols, MC simulations.

$\rho\sigma^3 = 7.5$. As we see from the data in Figure 9, the mean cluster size has increased further, and the cluster size distribution has become even narrower. This implies that the effective intercluster potential has become more repulsive with increasing ρ. Summarizing, two tendencies are clearly visible with increasing density: the position of the maximum of these curves, indicating the most probable cluster size, shifts to higher values while their width is reduced. This confirms on a more quantitative level the observations made at the beginning of this section that with increasing ρ the clusters become larger and more uniform in size.

In Figure 10, we plot the MC data for the mean value of n_c along an isotherm $k_BT/\epsilon = 1.1$ as a function of ρ for both the bcc and the fcc phase. These data are complemented by the theoretical prediction of DFT, where n_c is the value minimizing $f(n_c, \alpha)$ at a given state point. We see that n_c turns out to be proportional to the density. This has far-reaching consequences on the behavior of our system. Since $n_c = c\rho\sigma^3$, with c being a constant, the lattice constant a of the conventional cubic unit cell can be expressed as

$$\frac{a}{\sigma} = \left(\frac{\gamma n_c}{\rho\sigma^3}\right)^{1/3} = (\gamma c)^{1/3} = \text{const.} \qquad (18)$$

where $\gamma = 2$ for bcc and $\gamma = 4$ for fcc crystals. This shows that the lattice constant is density independent and does not change under compression, a behavior already predicted in ref 28 that has been put on a sound theoretical basis in ref 49. This means that, in striking contrast to harshly repulsive systems, the GEM-4 system does not react to an increase in density by diminishing its lattice constant. On the contrary, it is evidently more favorable for additional particles that are inserted into a fixed volume to join the clusters that have already formed at the lattice sites. We find that, for the GEM-4, $a_{bcc} \cong 1.58\sigma$ and $a_{fcc} \cong 2.00\sigma$. In ref 49, it has been argued that the emergence of this single length scale is set by q_*, the location of the negative minimum in $\tilde{\Phi}(q)$; that is, it is a property solely determined by the functional form of the interaction potential. Using the values of the lattice constants quoted above, we find it straightforward to show that the first nonvanishing RLVs of the bcc and fcc lattices have the magnitudes $\sigma K_{1,fcc} \cong 5.44$ and $\sigma K_{1,bcc} \cong 5.62$. Thus, both lie very close to the value $\sigma q_* \cong 5.57$, in agreement with the arguments put forward in ref 49. Within very good approximation, these values are constant at all densities, a feature that has also been seen in similar, two-dimensional models and has been termed the unwavering magnitude of the wave vector.[63] Finally, we point out that there is a discontinuity in n_c as the system undergoes a first-order transition from the bcc to the fcc phase (independent of its eventual exact location).

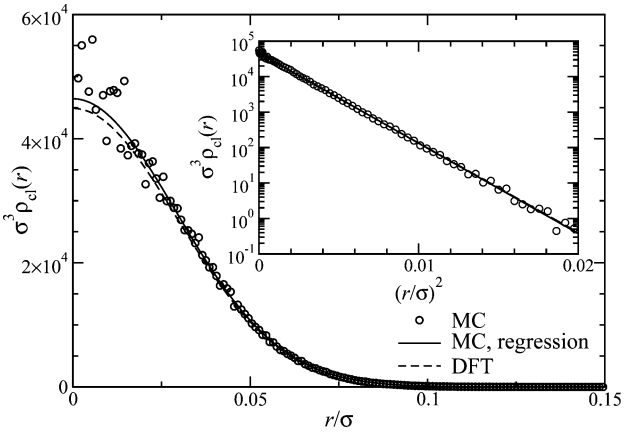

Figure 11. Cluster density profile $\rho_{cl}(r)$ of a cluster fcc crystal of the GEM-4 system at $k_BT/\epsilon = 0.1$ and $\rho\sigma^3 = 9$. The semilogarithmic plot of $\rho_{cl}(r)$ against r^2/σ^2 in the inset corroborates the Gaussian shape of the distribution.

Another characteristic feature of the system seen in Figure 9, namely, the tendency of the cluster size distribution to become narrower with increasing density, can be understood by the fact that a larger ρ brings about a concomitant growth in the energetic barrier separating particles on one lattice site from those occupying another, neighboring one. Thus, hopping between sites becomes prohibitively expensive, and the clusters tend to show reduced "polydispersity". In addition, the localization parameter α increases linearly with ρ; that is, the clusters become more compact as the density is increased. While the MC data for n_c nearly coincide with the DFT results, the agreement between the theoretical predictions for α and its corresponding value extracted from the simulations is slightly worse on quantitative grounds but is still excellent on a qualitative level. We point out that the linear dependence of both n_c and α on ρ has also been predicted in the theoretical framework of ref 49.

In Figure 11, we analyze the spherically averaged distribution $\rho_{cl}(r)$ of the particles inside a cluster. The state point we have chosen ($k_BT/\epsilon = 0.1$ and $\rho\sigma^3 = 9$) is taken from the region where the fcc cluster phase is definitely the stable one. Following the assumption made in eq 10, we fit the raw MC simulation data with a Gaussian shape for $\rho(r)$, with α and n_c as adjustable

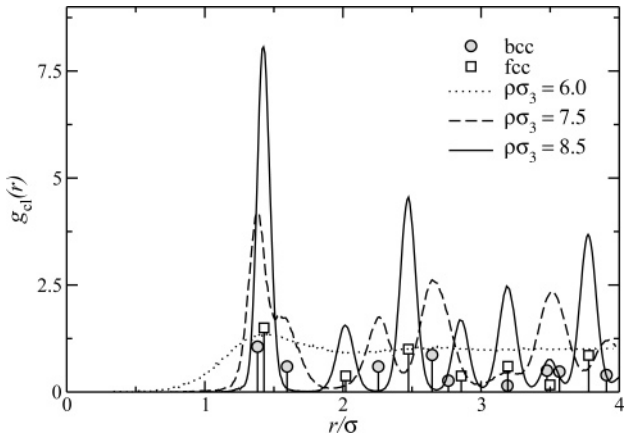

Figure 12. Radial distribution function $g_{cl}(r)$ of the centers of mass of the clusters for the three states of the GEM-4 system displayed in Figure 4 (i.e., at $k_BT/\epsilon = 1.1$). The markers indicate the positions of the neighboring shells of perfect bcc and fcc lattices, while the heights of the markers are proportional to the number of particles in the corresponding neighboring shells.

parameters. Though there might be slight differences at small r (where the statistics of MC is, as expected, poorest), the good qualitative agreement between simulation data and the fitted curve justifies a posteriori the assumption for the shape of the density profile $\rho(r)$ postulated in eq 10.

The excellent qualitative and the often even surprisingly good quantitative agreement between all MC and DFT results presented in this work provide a high level of confidence to the internal consistency of the underlying theoretical concept.

Because of the limitations of the MC simulations we use (constant box size and shape and fixed number of particles), phase transitions from bcc to fcc are highly unlikely to be observed. Still, spontaneous freezing of an initially liquid system as well as melting of a crystal during the course of a simulation have been observed. Thus, it is indispensable to unambiguously identify the crystalline structures within MC simulations. In Figure 12, we have calculated the RDF of the centers of mass of the clusters, that is, $g_{cl}(r)$, for the three systems shown in Figure 4. At $\rho\sigma^3 = 6$, that is, still in the fluid phase, $g_{cl}(r)$ shows a behavior that is typical for a fluid. At the higher densities, $\rho\sigma^3 = 7.5$ and $\rho\sigma^3 = 8$, the occurrence of pronounced peaks is yet another imprint of the fact that the clusters form regular solid structures. The fact that these peaks become more pronounced at higher densities corroborates once more our observation that the lattice structure is then less distorted and thus better defined. The positions of the markers in Figure 12 indicate the distances R_i^{fcc} or R_i^{bcc} of the different shells of neighbors around a central particle for the fcc or the bcc lattices. Their height is normalized analogously to the RDF and is proportional to the number of neighbors in the respective shell. As expected, for $\rho\sigma^3 = 7.5$, the positions of the peaks in $g_{cl}(r)$ coincide with the R_i^{bcc} of the bcc lattice, while for $\rho\sigma^3 = 8.5$, they coincide with the fcc ones, confirming that the initial structures did not melt or transform. Also, the height of the peaks of $g_{cl}(r)$ is correlated with the height of the respective markers. Thus, $g_{cl}(r)$ can serve as a clear indication of the respective crystalline structure of the systems.

As we have shown in Figure 11, the particles have a certain freedom to fluctuate around their equilibrium positions, that is, the perfect lattice sites, which can lead to slightly distorted crystals during the simulations. It is therefore convenient to find a more quantitative measure of the degree of crystallinity in our system, which has to fulfill several prerequisites: it has to be capable of unambiguously distinguishing between a liquid and the different crystalline phases, and it has to be insensitive to the orientation of the crystal in space. It was shown that the bond order parameters Q_4, Q_6, W_4, and W_6,[64,65] whose definitions are based on spherical harmonics, can be used as quantitative measures of cubic crystallinity, meeting all of the aforementioned requirements. In perfect cubic crystals, these parameters assume a unique value characteristic of the respective crystal structure. On the other hand, in a real crystal, these bond order parameters will have slightly different values at individual lattice sites, since the clusters fluctuate around their perfect positions. This leads to a distribution of bond order parameter values that can serve as a characteristic fingerprint of the different structures. Decomposing such a fingerprint to a linear combination of the corresponding distributions of known structures then allows for a quantitative determination of the structure of the system in the simulation box.[65] In the case of the MC simulations for the GEM-4 system, this tool has proven to be a reliable means to unambiguously distinguish between the liquid phase and the different hyper-crystals.

6. Conclusions

In this contribution, we have demonstrated that particles interacting via purely repulsive, bounded potentials and which have oscillating FTs are able to form stable clusters of overlapping particles. On the basis of investigations of the GEM-4 system, we show that the clustering phenomenon occurs both in the dense fluid and in the ordered, solid phases. In the fluid phase, these clusters are characterized by a broad distribution of cluster population. In the solid phases, which emerge from the fluid phase via first-order phase transitions, these clusters arrange themselves at the lattice sites of hyper-crystals. While the bcc structure is only stable in a narrow, wedge-like region of the (T, ρ) plane, the fcc cluster crystals are stable in the overwhelming part of phase space. Both freezing and melting lines are linear in the temperature range considered. In both solid phases, the respective lattice constant remains unchanged upon compression of the system, causing a linear growth with density of both the cluster population number and of the width of the approximately Gaussian distribution of particles inside a cluster. The properties of the fluid phase have been calculated in the MFA, while the solid cluster phases have been treated within classical DFT using a mean-field format, a simplification that has been justified in preceding theoretical considerations.[49] Complementing LMC simulations in the canonical ensemble provide data that are consistent with the DFT results. On the basis of investigations of the GEM-4 system, the present numerical work fully confirms the theoretical predictions made for $Q^{\pm}$ systems.

This new class of crystals also opens up a host of interesting questions regarding the dynamics of both individual particles and collective motions. For one, periodic solids with n_c particles per site can be seen as Bravais lattices with a basis; it is thus expected that they will feature phonon spectra with $3n_c$ acoustic branches and $3(n_c - 1)$ optical ones. The calculation of such spectra is challenging, especially as n_c grows. It is nevertheless a very interesting problem to see the evolution of the spectra with increasing n_c and to investigate the question whether these evolve with n_c following some systematic rules. At the same time, it makes no sense to speak about $3n_c$ phonon modes when n_c is a noninteger: there is a second type of excitation in the system, namely, "excess" particles that hop from one site to the other and bring about an arbitrary (noninteger) occupancy n_c. Recent results[66] indicate that the hopping processes bring

about a long-time diffusivity D in such periodic crystals, with $D \sim \exp(-A\rho/T)$, A being some constant. A concerted effort to understand those processes via analytical approaches and simulation is under way. The combined effects of phonons and hopping, the appearance of possible phononic gaps in the material,[67] and the ways to tune those will be the subject of future work.

Acknowledgment. The authors thank Daan Frenkel for many helpful discussions. B.M.M., D.G., and G.K. acknowledge financial support by the Österreichische Forschungsfond (FWF) under Project Nos. P19890-N16 and P17823-N08 and by the Hochschuljubiläumsstiftung der Stadt Wien under Project No. 1080/2002. Furthermore, B.M.M. thanks the Österreichische Forschungsgemeinschaft for financial support. This work was partly carried out under the HPC-EUROPA Project (RII3-CT-2003-506079), with the support of the European Community-Research Infrastructure Action under the FP6 "Structuring the European Research Area" Programme. C.N.L. acknowledges partial support from the Deutsche Forschungsgemeinschaft within the Collaborative Research Center SFB-TR6, Project Section C3.

References and Notes

(1) Sear, R. P.; Gelbart, W. M. *J. Chem. Phys.* **1999**, *110*, 4582.
(2) Sciortino, F.; Mossa, S.; Zaccarelli, E.; Tartaglia, P. *Phys. Rev. Lett.* **2004**, *93*, 055701.
(3) Mossa, S.; Sciortino, F.; Tartaglia, P.; Zaccarelli, E. *Langmuir* **2004**, *20*, 10756.
(4) Campbell, A. I.; Anderson, V. J.; van Duijneveldt, J. S.; Bartlett, P. *Phys. Rev. Lett.* **2005**, *94*, 208301.
(5) Sanchez, R.; Bartlett, P. *J. Phys.: Condens. Matter* **2005**, *17*, S3351.
(6) Imperio, A.; Reatto, L. *J. Phys.: Condens. Matter* **2004**, *16*, S3769.
(7) Imperio, A.; Reatto, L. *J. Chem. Phys.* **2006**, *124*, 164712.
(8) Likos, C. N.; Mayer, C.; Stiakakis, E.; Petekidis, G. *J. Phys.: Condens. Matter* **2005**, *17*, S3363.
(9) Stiakakis, E.; Petekidis, G.; Vlassopoulos, D.; Likos, C. N.; Iatrou, H.; Hadjichristidis, N.; Roovers, J. *Europhys. Lett.* **2005**, *72*, 664.
(10) Sear, R. P.; Frenkel, D. *Phys. Rev. Lett.* **2003**, *90*, 195701.
(11) Charbonneau, P.; Reichman, D. R. *Phys. Rev. E* **2007**, *75*, 011507.
(12) Charbonneau, P.; Reichman, D. R. *Phys. Rev. E* **2007**, *75*, 050401-(R).
(13) Klein, W.; Gould, H.; Ramos, R. A.; Clejan, I.; Mel'cuk, A. I. *Physica A* **1994** , *205*, 738.
(14) Krüger, B.; Schäfer, L.; Baumgärtner, A. *J. Phys. (France*) **1989**, *50*, 319.
(15) Dautenhahn, J.; Hall, C. K. *Macromolecules* **1994**, *27*, 5399.
(16) Louis, A. A.; Bolhuis, P. G.; Hansen, J.-P.; Meijer, E. J. *Phys. Rev. Lett.* **2000**, *85*, 2522.
(17) Götze, I. O.; Harreis, H. M.; Likos, C. N. *J. Chem. Phys.* **2004**, *120*, 7761.
(18) Ballauff, M.; Likos, C. N. *Angew. Chem., Int. Ed.* **2004**, *43*, 2998.
(19) Denton, A. R. *Phys. Rev. E* **2003**, *67*, 011804; erratum, *68*, 049904.
(20) Gottwald, D.; Likos, C. N.; Kahl, G.; Löwen, H. *Phys. Rev. Lett.* **2004**, *92*, 068301.
(21) Gottwald, D.; Likos, C. N.; Kahl, G.; Löwen, H. *J. Chem. Phys.* **2005**, *122*, 074903.
(22) Pierleoni, C.; Addison, C.; Hansen, J.-P.; Krakoviack, V. *Phys. Rev. Lett.* **2006**, *96*, 128302.
(23) Hansen, J.-P.; Pearson, C. *Mol. Phys.* **2006**, *104*, 3389.
(24) Likos, C. N. *Phys. Rep.* **2001**, *348*, 267.
(25) Stillinger, F. H.; Stillinger, D. K. *Physica A* **1997**, *244*, 358.
(26) Lang, A.; Likos, C. N.; Watzlawek, M.; Löwen, H. *J. Phys.: Condens. Matter* **2000**, *12*, 5087.
(27) Watzlawek, M.; Likos, C. N.; Löwen, H. *Phys. Rev. Lett.* **1999**, *82*, 5289.
(28) Likos, C. N.; Lang, A.; Watzlawek, M.; Löwen, H. *Phys. Rev. E* **2001**, *63*, 031206.
(29) Stillinger, F. H. *J. Chem. Phys.* **1976**, *65*, 3968.
(30) Stillinger, F. H.; Weber, T. A. *J. Chem. Phys.* **1978**, *68*, 3837.
(31) Stillinger, F. H.; Weber, T. A. *Phys. Rev. B* **1980**, *22*, 3790.
(32) Prestipino, S.; Saija, F.; Giaquinta, P. V. *Phys. Rev. E* **2005**, *71*, 50102.
(33) Stillinger, F. H. *J. Chem. Phys.* **1979**, *70*, 4067.
(34) Stillinger, F. H. *Phys. Rev. B* **1979**, *20*, 299.
(35) Evans R. In *Density Functionals in Nonuniform Fluids, in: Fundamentals of Inhomogeneous Fluids*; Henderson, D., Ed.; Marcel Dekker: New York, 1992.
(36) Baus, M. *J. Phys.: Condens. Matter* **1990**, *2*, 2111.
(37) Louis, A. A; Bolhuis, P. G.; Hansen, J.-P. *Phys. Rev. E* **2000**, *62*, 7961.
(38) Likos, C. N.; Watzlawek, M.; Löwen, H. *Phys. Rev. E* **1998**, *58*, 3135.
(39) Fernaud, M.-J.; Lomba, E.; Lee, L. L. *J. Chem. Phys.* **2000**, *112*, 810.
(40) Schmidt, M. *J. Phys.: Condens. Matter* **1999**, *11*, 10163.
(41) Rosenfeld, Y.; Schmidt, M.; Watzlawek, M.; Löwen, H. *Phys. Rev. E* **2000**, *62*, 5006.
(42) Acedo, L.; Santos, A. *Phys. Lett. A* **2004**, *323*, 427.
(43) Santos, A. *Mol. Phys.* **2006**, *104*, 3411.
(44) Malijevský, A.; Santos, A. *J. Chem. Phys.* **2006**, *124*, 074508.
(45) Santos, A.; Malijevský, A. *Phys. Rev. E* **2007**, *75*, 021210; **2007**, *75*, 049901(E).
(46) Malijevský, A.; Yuste, S. B.; Santos, A. *eprint arXiv:cond-mat/0705.1069*.
(47) Mladek, B. M.; Gottwald, D.; Kahl, G.; Neumann, M.; Likos, C. N. *Phys. Rev. Lett.* **2006**, *96*, 045701; erratum, *97*, 019901.
(48) Fragner, H. *Phys. Rev. E* **2007**, *75*, 061402.
(49) Likos, C. N.; Mladek, B. M.; Gottwald, D.; Kahl, G. *J. Chem. Phys.* **2007**, *126*, 224502.
(50) Likos, C. N.; Hoffmann, N.; Löwen, H.; Louis, A. A. *J. Phys.: Condens. Matter* **2002**, *14*, 7681.
(51) Mladek, B. M.; Kahl, G.; Likos, C. N., arXiv:0708.4380.
(52) Hansen, J.-P.; McDonald, I. R. *Theory of Simple Liquids*, 3rd ed.; Elsevier: Amsterdam, 2006.
(53) Gottwald, D.; Kahl, G.; Likos, C. N. *J. Chem. Phys.* **2005**, *122*, 204503-1.
(54) Fragner H. Lattice Monte Carlo Simulation mit rekonfigurierbaren Prozessoren, Ph.D. Thesis, University of Vienna, 2005.
(55) Fragner, H. *Comput. Phys. Commun.* **2007**, *176*, 327.
(56) Panagiotopoulos, A. Z. *J. Chem. Phys.* **2000**, *112*, 7132.
(57) Frenkel, D.; Smit, B. *Understanding Molecular Simulation*, 2nd ed.; Adacemic Press: London, 2002.
(58) Hansen, J.-P.; Verlet, L *Phys. Rev.* **1969**, *84*, 151.
(59) Hansen, J.-P.; Schiff, D. *Mol. Phys.* **1973**, *25*, 1281.
(60) Mladek, B. M.; Fernaud, M.-J.; Kahl, G.; Neumann, M. *Condens. Matter Phys.* **2005**, *8*, 135.
(61) Widom, B. *J. Chem. Phys.* **1963**, *39*, 2802.
(62) Mladek, B. M.; Charbonneau, P.; Frenkel D., arXiv:0708.2979.
(63) Glaser, M. A.; Grason, G. M.; Kamien, R. D.; Kosmrlj, A.; Santagelo, C. D.; Ziherl, P. *Europhys. Lett.* **2007**, *78*, 46004.
(64) Steinhardt, P. J.; Nelson, D. R.; Ronchetti, M. *Phys. Rev. B* **1983**, *28*, 784.
(65) ten Wolde, P. R.; Ruiz-Montero, M. J.; Frenkel, D. *Phys. Rev. Lett.* **1995**, *75*, 2714; *J. Chem. Phys.* **1996**, *104*, 9932.
(66) Moreno, A.; Likos, C. N. *Phys. Rev. Lett.* **2007**, *99*, 107801.
(67) Cheng, W.; Wang, J.; Jonas, U.; Fytas, G.; Stefanou, N. *Nat. Mater.* **2006**, *5*, 830.